

Basaltic glass formed from hydrovolcanism and impact processes: Characterization and clues for detection of mode of origin from VNIR through MWIR reflectance and emission spectroscopy



W.H. Farrand^{a,*}, S.P. Wright^b, A.D. Rogers^c, T.D. Glotch^c

^aSpace Science Institute, 4750 Walnut Street, Suite 205, Boulder, Colorado 80301, USA

^bPlanetary Science Institute, 1700 E. Ft. Lowell Rd., #106, Tucson, AZ 85719, USA

^cDepartment of Geosciences, Stony Brook University, 255 Earth and Space Sciences Building, Stony Brook, NY 11794, USA

ARTICLE INFO

Article history:

Received 30 December 2015

Revised 1 March 2016

Accepted 28 March 2016

Available online 8 April 2016

Keywords:

Mars, surface

Volcanism

Impact processes

Spectroscopy

Mineralogy

ABSTRACT

The CheMin X-ray diffraction instrument on-board the Curiosity rover in Gale crater has measured a consistent X-ray amorphous component in drill core samples examined to-date, clearly demonstrating that X-ray amorphous materials are a significant fraction of the martian surface layer. Glasses are potential components of this amorphous material and in this study, basaltic tephra from several hydro- and glaciovolcanic centers, as well as impact melts from India's Lonar Crater, were examined using thin section petrography, visible and near-infrared reflectance and mid-wave infrared emission spectroscopy as well as measuring major and minor element chemistry of representative samples using X-ray fluorescence (XRF) spectroscopy. The objectives of this study have been to look for distinguishing characteristics between volcanic and impact glasses and to determine features that indicate whether the glasses are fresh or altered using methods available on current and planned Mars rovers. Spectral features in the visible and near-infrared (VNIR) that can be used as indicators of alteration include the development of hydration features at 1.9 and $\sim 3 \mu\text{m}$ and a feature attributed to ferric oxide development at $0.48 \mu\text{m}$. In the mid-wave infrared, it was observed that glass-rich tephra field samples did not display a broad, disordered glass feature near 9–10 μm (as is observed in pristine basaltic glasses) but rather a doublet with centers near 9.5 and 11 μm attributed in earlier work to incipient devitrification into SiO_4 chain and sheet structures respectively. A tentative observation was made that the Si–O bending feature, observed in all the sample spectra near 22 μm was broader in the hydro- and glaciovolcanic glass samples than in the impact glass samples. Hydro- and glaciovolcanic glass-rich tephra samples were used as library spectra in linear deconvolution analyses of Mars Global Surveyor Thermal Emission Spectrometer (MGS TES) surface spectral types. These incipiently devitrified glass spectra were selected for all of the surface types and formed close to 40% of the N. Acidalia Planitia spectral type.

© 2016 Elsevier Inc. All rights reserved.

1. Introduction

It has been recognized in recent years that the martian surface layer contains a substantial component of amorphous materials. Such materials exist both in the unconsolidated regolith and in many rocks examined by Mars rovers. Observations by the MGS TES instrument suggested significant fractions (10–20%) of poorly crystalline or amorphous materials in low-dust regions of Mars (Rogers and Christensen, 2007). Observations by the Mini-TES instrument on the Mars Exploration Rover Spirit detected the presence of high fractions of glass in rocks across the Hus-

band Hill region and in the Home Plate feature (Ruff et al., 2006; 2008; Schmidt et al., 2009). Curiosity's CheMin XRD instrument has found a significant component of amorphous materials in all the targets analyzed to date (Downs et al., 2015). Horgan and Bell (2012) also suggested on the basis of analysis of orbital OMEGA data that glass is present as a significant component of the northern plains of Mars.

For glasses, and very likely for other poorly crystalline materials that might be early alteration products of glasses, the question arises: what is the origin of the glass? Glass can be formed both through volcanic and impact processes. Are there discernible chemical or spectral differences in terrestrial examples of volcanic and impact glasses that could then be sought in examples of martian glasses? The chemical or spectral properties to be examined should be those detectable from instruments on existing or

* Corresponding author. Tel.: +1 720 974 5825.

E-mail address: Farrand@spacescience.org (W.H. Farrand).

Table 1
Field sites from which samples were collected.

Field site	Mode of formation	Sample abbreviation
N. Menan Butte, Idaho	Hydrovolcanic tuff cone	NMB
Sinker Butte, Idaho	Hydrovolcanic tuff cone	SB
White Butte, Idaho	Subaqueous tuff cone	WhB
Split Butte, Idaho	Hydrovolcanic tuff ring	SplB
Pavant Butte, Utah	Hydrovolcanic tuff cone	PB
Crazy Hills, Washington	Glaciovolcanic hyaloclastite ridge	CH
Helgafell, Iceland	Glaciovolcanic hyaloclastite ridge	Hf
Lunar Crater, India	Impact crater	LC

Table 2
Thin section point count results.

Sample	Thin section point count percentages (adjusted for voids)
NMB12-01	Glass = 81%, Groundmass/tachylite = 9%, Plagioclase < 1%, Mafic Xls = 4%, Opaques = 4%, Palagonite = 2%
NMB12-02	Glass = 70%, Groundmass/tachylite = 9%, Plagioclase = 1%, Mafic Xls = 2%, Opaques = 18%, Palagonite = 1%
NMB12-09	Glass = 54%, Groundmass/tachylite = 35%, Plagioclase < 1%, Mafic Xls = 1%, Opaques = 9%, Palagonite < 1%, Zeolites < 1%,
NMB12-14	Glass = 77%, Groundmass/tachylite = 12%, Plagioclase < 1%, Mafic Xls = 1%, Opaques = 8%, Palagonite < 1%
CH-02	Glass = 81%, Groundmass/tachylite = 14%, Plagioclase = 2%, Mafic Xls < 1%, Opaques = 2%, Palagonite < 1%
Hf-01	Glass = 60%, Groundmass/tachylite = 4%, Plagioclase < 1%, Mafic Xls = 1%, Opaques = 14%, Palagonite = 18%
Hf-06	Glass = 75%, Groundmass/tachylite = 11%, Plagioclase < 1%, Mafic Xls < 1%, Opaques = 6%, Palagonite = 7%
PB13-004A	Glass = 55%, Groundmass/tachylite = 26%, Plagioclase = 4%, Mafic Xls = 4%, Opaques = 6%, Zeolites = 6%

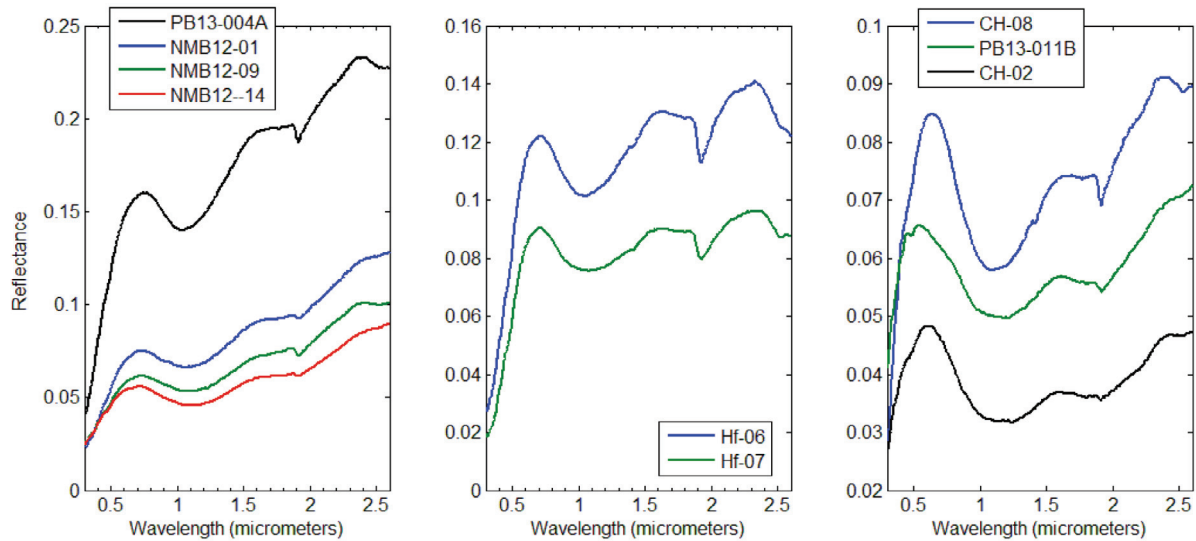


Fig. 1. Bidirectional reflectance of hydro- and glaciovolcanic basaltic glasses. Spectra have not been offset, but note changes in vertical scale.

planned Mars rovers and/or orbiting spacecraft. While other studies have examined artificial glasses (Minitti et al., 2002, Minitti and Hamilton, 2010), in this study, we have examined samples of naturally formed glasses of basaltic composition generated through hydrovolcanic and glaciovolcanic activity and also impact-generated glasses from India's Lunar crater which was formed in the vast Deccan flood basalts (Fredriksson et al., 1973). The methods of examination have included measurements analogous to those available from past or operating Mars rovers (Spirit, Opportunity, and Curiosity) or planned for future rovers (ExoMars, Mars 2020). These include visible and near infrared (VNIR) reflectance, thermal infrared (TIR) emissivity, major and trace element chemistry, and X-ray diffraction (XRD). We have also examined thin sections of these samples and have collected 2.5–25 μm specular reflectance over individual grains using a micro-FTIR instrument.

Primary field sites for this study included centers of water-magma interaction in the American west including sites on the Snake River Plain of Idaho—principally N. Menan Butte (Creighton, 1987), Sinker Butte (Brand and White, 2007), and Split Butte (Womer, 1977). We also worked at the Pavant Butte (spelled as

“Pahvant Butte” on some maps) tuff cone that erupted into glacial Lake Bonneville (White, 1996; Wohletz and Sheridan, 1983) in Utah. Samples previously collected from glaciovolcanic (ice-magma interaction) sites—namely the Lone Butte and Crazy Hills region in southern Washington state (Hammond, 1987) and the Helgafell hyaloclastite ridge in Iceland (Schopka et al., 2006) were also examined. The impact glasses examined are from Lunar crater in India (Fredriksson et al., 1973; Maloof et al., 2010). A summary of field sites, their mode of formation, and abbreviations for samples from those sites is provided in Table 1.

2. Methodology

2.1. Visible and near infrared reflectance

Bidirectional reflectance of select powdered samples from 0.3 to 2.6 μm and biconical reflectance from 0.8 to 25 μm was measured at the Reflectance Experiment Laboratory (RELAB) at Brown University (Pieters et al., 1996). Reflectance measurements provide information on mineralogy derived from electronic charge

transfer and crystal field bands in the visible to near infrared and from vibrational overtones and vibrational fundamental bands in the short-wave and mid-wave infrared (e.g., Clark, 1999). Bulk samples measured were ground with a stainless steel mortar and pestle to less than a 400 μm sieve spacing and reflectance was measured of these powdered samples.

2.2. Thermal emissivity

Thermal emission spectra of bulk hand samples were collected using similarly configured instruments at Arizona State University, Stony Brook University, and at the Southwest Research Institute in Boulder, Colorado. Sample measurement and spectral calibration procedures followed Ruff et al. (1997). The spectra collected were resampled to match the 923 channel wavenumber set of the ASU spectrometer covering the spectral range of 2000–220 cm^{-1} (5–45 μm).

2.3. Petrography and micro-FTIR

Thin sections were prepared of a number of samples. Thin sections were visually inspected using a petrographic microscope. Point counting results for glass-rich samples from which thin sections were prepared are shown in Table 2. In all but one sample discussed here, there were 2% or less plagioclase and mafic phases (olivine and pyroxene). Opaque minerals, attributed to Fe oxides, are spectrally neutral at wavelengths less than 14 μm . The effect of alteration (resulting in the formation of phases including palagonite and zeolites) is addressed below by examining the strength of spectral features in the VNIR associated with oxidation and hydration.

Uncovered thin sections were examined at the Stony Brook University Vibrational Spectroscopy Laboratory using a Nicolet iN10MX FTIR microscope with a liquid nitrogen cooled Hg-Cd-Te 16 pixel linear array detector. This instrument was used to collect hyperspectral image cubes (in reflectance) of portions of a number of the thin sections between 4000 and 715 cm^{-1} . (2.5–14 μm). Select point spectra were also collected over the broader range of 4000–400 cm^{-1} (2.5–25 μm) using an uncooled single pixel deuterated triglycine sulfate (DTGS) detector. The spatial resolution of the hyperspectral image cubes is 25 μm /pixel, while individual DTGS measurements can range from 50 \times 50 μm to 400 \times 400 μm .

2.4. X-Ray fluorescence determined major and minor element chemistry

XRF measurements of samples of relatively unaltered as well as altered volcanic and impact glasses were made by Dr. S. A. Mertzman of Franklin & Marshall College. In addition to major element chemistry, information on trace elements Rb, Sr, Y, Zr, Nb, Ni, Ga, Cu, Zn, U, Th, Co, Pb, Sc, Cr, V, La, Ce, and Ba were obtained. Also measured were loss-on-ignition (LOI) and relative proportions of FeO and Fe_2O_3 via FeO titration.

3. Observations

3.1. VNIR reflectance

Fig. 1 shows 0.3–2.6 μm bidirectional reflectance spectra of several hydro- and glaciovolcanic glass-rich samples. As described in past research (e.g., Farrand, 1991; Farrand and Singer, 1992) these spectra have low reflectance and broad glass bands centered from 1.05 to 1.15 μm and in the vicinity of 1.97 μm . This correlates well with the glass band absorptions noted by Dyar and Burns (1982) centered between 1.0 and 1.05 μm and between 1.7 and 1.9 μm . These absorptions are attributed respectively to crystal

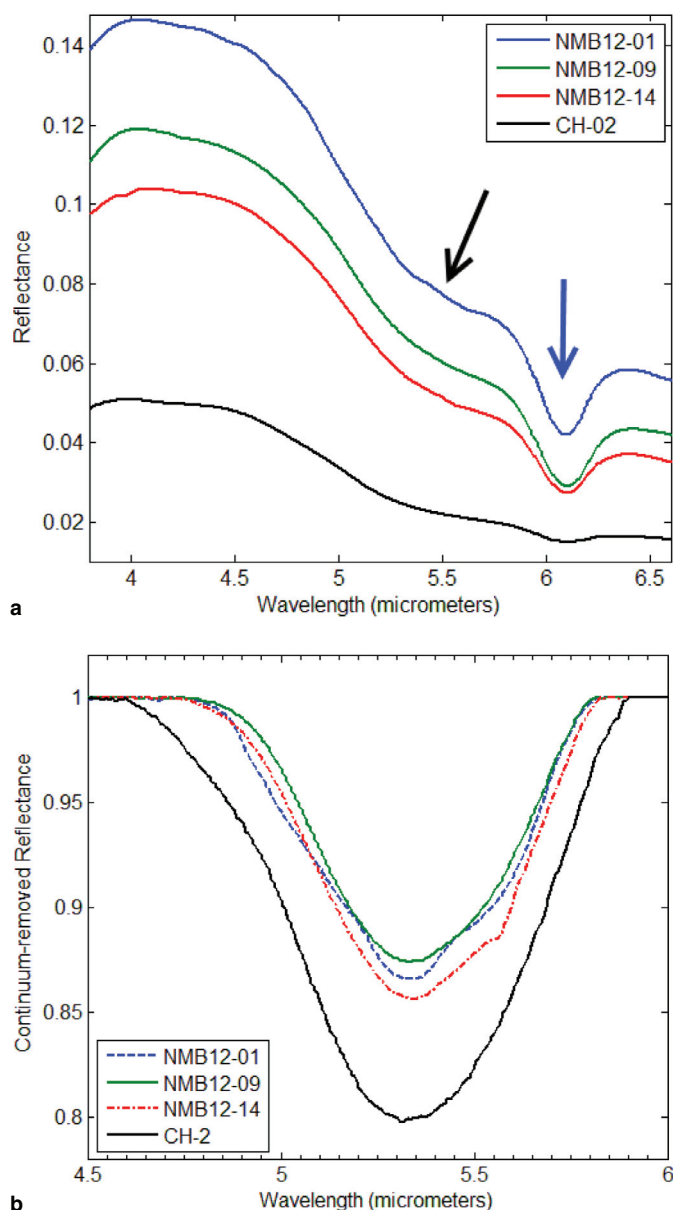


Fig. 2. (A) 3.8–6.6 μm reflectance of glassy samples from Fig. 1. Blue arrow indicates 6.1 μm water band. Black arrow indicates 5.3 μm glass band. (B) Continuum-removed spectra from Fig. 2A highlighting 5.3 μm glass band. Continuum-removed from 4.4 to 6 μm .

field transitions in octahedrally coordinated Fe^{2+} ions and tetrahedrally coordinated Fe^{2+} ions in the glass (Dyar and Burns, 1982). The exact centers of the “2 μm ” band in our samples are difficult to determine since there is a weak 1.92 μm bound water overtone band in all of the spectra. The presence of the 1.92 μm band in even very low reflectance materials is an indicator of how even very black, fresh appearing materials can exhibit some level of hydration in their spectra.

At wavelengths beyond 2.6 μm in the biconical reflectance spectra, an additional glass spectral feature is observable in spectra with a linear continuum removed from 4 to 6 μm in the form of a broad band centered at approximately 5.32 μm (Fig. 2a). We attribute this band to the Si–O overtone combination band noted by King et al. (2004). This band is strongest in the darkest, least altered CH-2 sample spectrum (Fig. 2b).

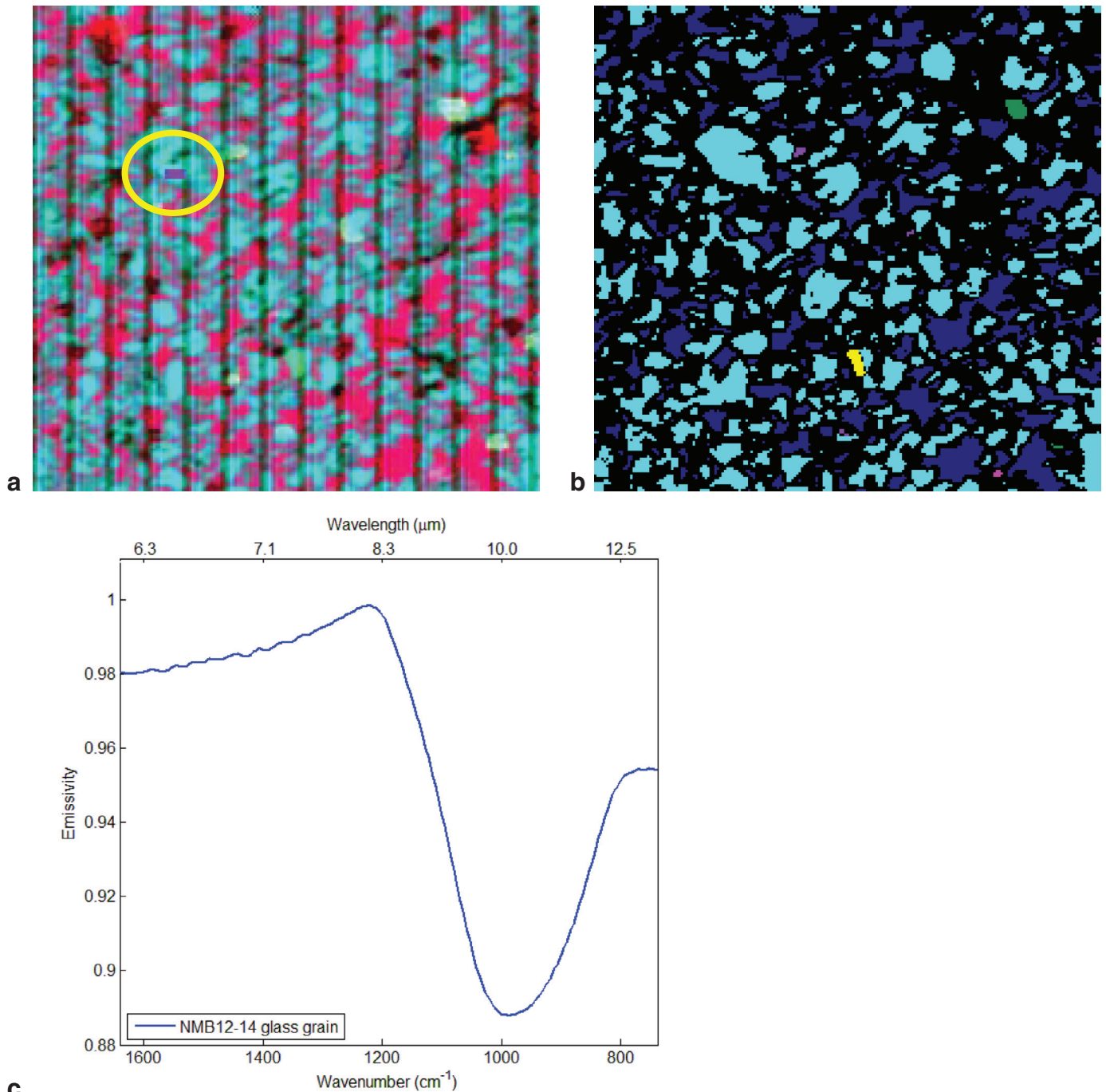


Fig. 3. **A.** Composite of 1250, 950, and 750 cm^{-1} bands of a portion of a NMB12-14 thin section viewed in the Vibrational Spectroscopy Lab's micro-FTIR. Yellow ellipse surrounds glass grain from which region of interest average spectrum, marked in purple, in Fig. 3C was extracted. **B.** SAM (Spectral Angle Mapper) class map of NMB12-14 micro-FTIR scene. Cyan=glass, yellow=plagioclase, purple=pyroxene, green=olivine, dark blue=epoxy filled voids, black=unclassified. **C.** Extracted average region of interest spectrum from the NMB12-14 micro-FTIR observation. (For interpretation of the references to colour in this figure legend, the reader is referred to the web version of this article.)

3.2. TIR sample emissivity and micro-FTIR analyses

Micro-FTIR analysis allows for the examination of the Mid-Wave Infrared (MWIR) reflectance of individual glass grains in thin section (Fig. 3a). These values were translated to emissivity via Kirchoff's Law (emissivity = 1 – reflectance, assuming transmittance = 0; e.g., an opaque surface) for more ready comparison to bulk sample emissivity measurements. We note that Kirchoff's Law is only strictly true for an isothermal system. Thus, laboratory measured emissivity data are most directly relatable

to remotely sensed data (e.g., Christensen et al., 2000). The 4–14 μm (2500–714 cm^{-1}) reflectance of glass grains display the broad “U” shaped absorption (Fig. 3c) described in past studies of fresh basaltic glass (e.g., Crisp et al., 1990; Minitti et al., 2002; Minitti and Hamilton, 2010). The SiO_4 stretching absorption responsible for the feature shown in Fig. 3c has an emissivity minimum that varies somewhat between samples but has a median minimum position at 10.13 μm (987.4 cm^{-1}). The hyperspectral image cubes measured by the Micro-FTIR were mapped using hyperspectral mapping approaches such as spectral

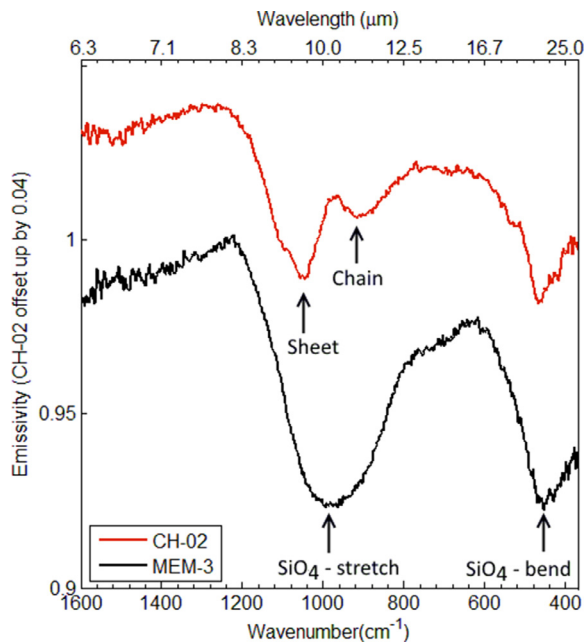


Fig. 4. Comparison of pristine basaltic glass spectrum MEM-3 (black) and partially devitrified glaciovolcanic glass CH-02 (red). Absorption features discussed in the text are labeled. (For interpretation of the references to colour in this figure legend, the reader is referred to the web version of this article.)

mixture analysis (Adams et al., 1993) and spectral angle mapping (Fig. 3b; Kruse et al., 1993).

The emissivity spectra of even the “freshest” (samples with the lowest reflectance and weakest 1.92 μm hydration band) bulk samples of glass-rich tephra have a distinctly different shape in the 8–14 μm region from that of the individual glass grains observed in the micro-FTIR data and from previously reported spectra of fresh basaltic glass. This difference is shown in Fig. 4 in a comparison between a fresh basaltic glass spectrum from the ASU spectral library (Christensen et al., 2000) and a fresh appearing glass-rich tephra from the Crazy Hills hyaloclastite ridge (sample CH-02). Additional examples of the differences in the natural samples are shown in Fig. 5a for RELAB-measured reflectance spectra (converted to emissivity) and sample spectra measured in emissivity shown in Fig. 5b. Labeled in Fig. 4 are the silicate stretching absorption of the pristine glass at 10.1 μm (990 cm⁻¹) and the silicate bending absorption at approximately 22 μm (454 cm⁻¹) (Farmer, 1974). However, the partially devitrified glass-rich hydrovolcanic samples display a doublet with a narrow emissivity band with a minimum at approximately 9.5–9.6 μm (1052.6–1041.7 cm⁻¹) and a broader shoulder centered at approximately 10.9–11.3 μm (917.4–885 cm⁻¹). These features are located in the region of silicate stretching vibrations (Farmer, 1974) and correspond to the “B” and “C” features of basaltic glasses from Hawaiian lava flows described by Crisp et al. (1990). Those authors described how the broad “U” shaped feature of fresh basaltic glass centered at approximately 9.96–10.2 μm (1004–979 cm⁻¹) changes into these features as disordered silica tetrahedra start to become ordered into *chains* of silica tetrahedra (causing the 10.9–11.3 μm or “C” feature) and *sheets* of silica tetrahedra (causing the 9.5–9.6 μm or “B” feature). Henceforth we refer to these respectively as the “SiO₄-chain” and “SiO₄-sheet” features. According to Crisp et al. (1990), the SiO₄-chain feature is initially stronger, but with time it weakens and the SiO₄-sheet feature becomes stronger. In all of the minimally altered, glass-rich hydrovolcanic samples examined here, the SiO₄-sheet feature is stronger than the SiO₄-chain feature. From sample to sample however, the latter feature can take the form of either a

weak band with a resolvable emissivity minimum, a shoulder, or just an expression of asymmetry in a “V” shaped absorption (as in the Hf-07 spectrum of Fig. 5B and Hf-06 in Fig. 7). The emissivity spectra of bulk samples also display a band with a minimum from 470 to 450 cm⁻¹ (21.3 to 22.2 μm), which corresponds to the region of silicate bending vibrations (Farmer, 1974).

As described by Crisp et al. (1990), the SiO₄-chain and sheet features developed initially in a very thin (suggested by Crisp et al., 1990 to be only 1–2 μm thick) rind on the glassy basalts examined in that study. This explains the disparity between the micro-FTIR spectra of the glass grains, which display the broader, U-shaped glass band and the bulk sample emissivity spectra in which that band has evolved into the dual SiO₄-chain and sheet features. In the former case, thin sections were being examined, thus any alteration rind was removed in the process of making the thin section. In the latter case, the bulk samples were relatively undisturbed from their collection locale in the field and thus any alteration rind was preserved. This effect is further illustrated in Fig. 6 in which the emissivity of a relatively undisturbed portion of the NMB12-14 sample is compared with that of the billet of the NMB12-14 sample left over from thin section preparation. The latter has the more “U” shaped band and the former has the dual SiO₄-chain and sheet features. However, while more “U” shaped, the NMB12-14 billet spectrum still shows an asymmetry with a minimum at 10.1 μm (989.3 cm⁻¹) which is different from the more symmetrical glass grain spectrum of Fig. 3C and the fresh glass spectrum in Fig. 4. As is also apparent in Fig. 6, the SiO₄ bending band appears with a similar shape in both the bulk sample and the cut surface of the same sample.

Glaciovolcanic samples from the Helgafell hyaloclastite ridge lack any sort of well-defined SiO₄-chain feature. Its manifestation is only as an asymmetry in the silica-stretching feature (Fig. 7). A cut surface of the glass-rich Hf-06 sample (75% glass from thin section point counts) shows the more “U” shaped band of pristine basaltic glasses.

3.2.1. Linkages between spectral features and geochemistry

The samples discussed here were selected on the basis of their being the least altered and most glass-rich samples with that initial assessment made on the basis of relative level of reflectance (less altered samples being lower in reflectance) and on the thin section point counts (Table 2). However, other spectral features can be used as indicators of the relative level of alteration and can be used to find those samples that are truly the least affected by alteration. As noted above, the samples display weak 1.9 and 6.1 μm bands evidencing incipient hydration caused by, respectively, combinations of the H–O–H bend with O–H stretches and the H–O–H bending vibration. The samples also display evidence of oxidation as indicated by weak Fe³⁺ features, notably a 0.48 μm band. This correlates with the feature described by Minitti et al. (2002) that they noted as developing with oxidation and which they attributed to hematite. As the 0.48 μm band strengthens, the shallow 5.3 μm glass band becomes progressively weaker as indicated in Fig. 8 for band depths of these features for hydro- and glaciovolcanic glass-rich samples.

The degree of oxidation can also be compared against the degree of hydration by plotting 0.48 μm band depth versus 6 μm band depth as shown in Fig. 9. Comparing the samples in these plots, the WhB12-05, CH-02 and PB13-011B have the strongest 5.3 μm glass bands and weakest 0.48 μm bands, followed by the N. Menan Butte samples (NMB12-01, 09, 14). However, in the plot of 0.48 μm band depth versus 6 μm band depth, WhB12-05 has the strongest 6 μm band depth and NMB12-09 also has a higher 6 μm band depth than the other N. Menan Butte glass-rich samples. In both plots, Hf-07 displays features indicative of greater alteration than the other samples with high 0.48 μm and 6 μm band depth

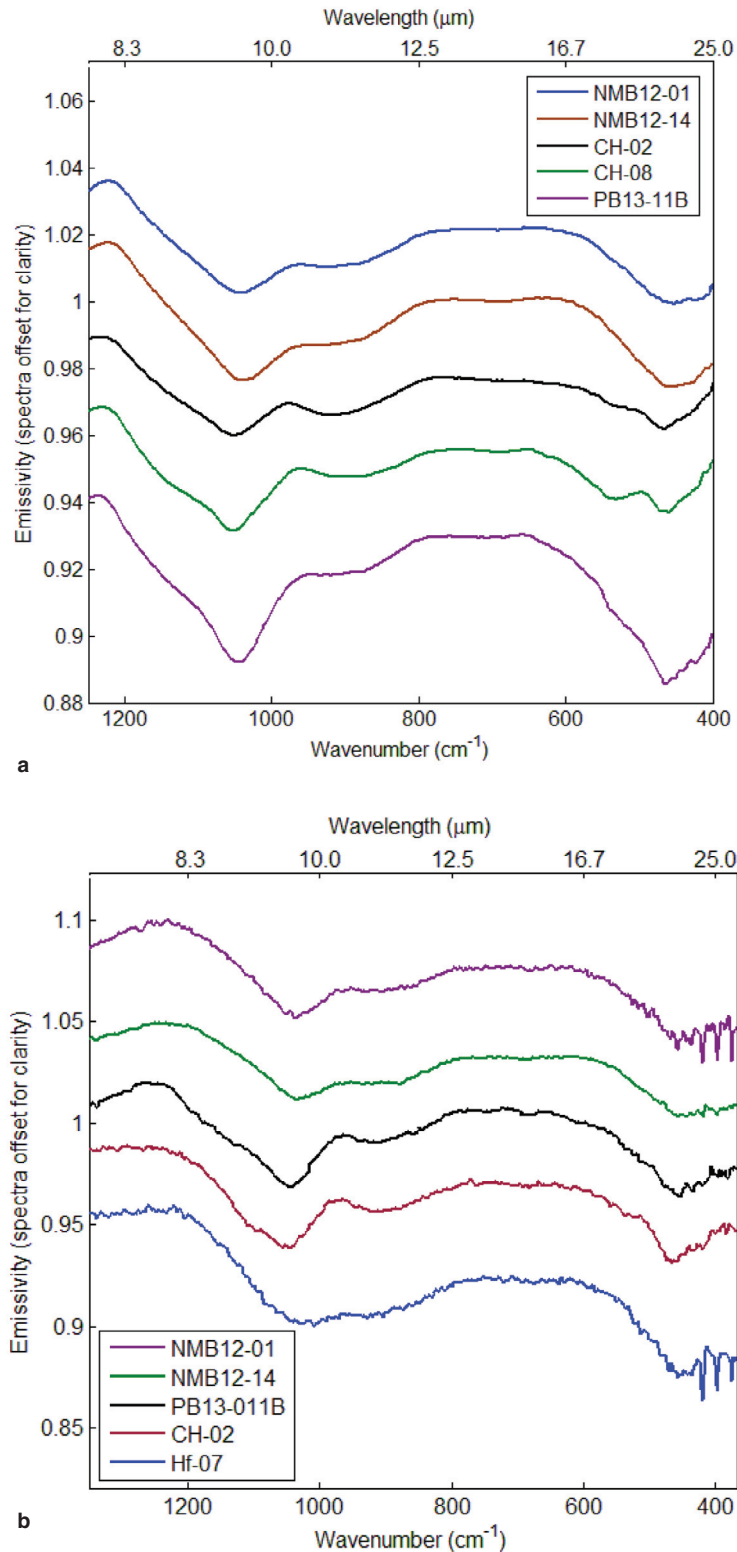


Fig. 5. A. Reflectance spectra converted to emissivity (and plotted with wavenumber on a linear scale) of several glass-rich samples showing “V” shaped “B” feature near $9.5\ \mu\text{m}$ and “C” feature centered from 10.9 to $11.2\ \mu\text{m}$. B. Emissivity spectra of bulk glass-rich samples. (For interpretation of the references to colour in this figure legend, the reader is referred to the web version of this article.)

and low $5.3\ \mu\text{m}$ band depth. Thus, on the basis of the relative weakness of the above spectral features, and the relative strength of the $5.3\ \mu\text{m}$ band, CH-02, PB13-011B are the least hydrated and oxidized and most glassy with NMB12-14 being next in that order.

The positions of the emissivity minima of the features described above vary from sample-to-sample. Specifically, the minima of the SiO_4 -chain features have a direct correlation with SiO_2 content of the samples. This is illustrated in Fig. 10 with a plot of % SiO_2 versus the minimum in wave number space of the SiO_4 -chain

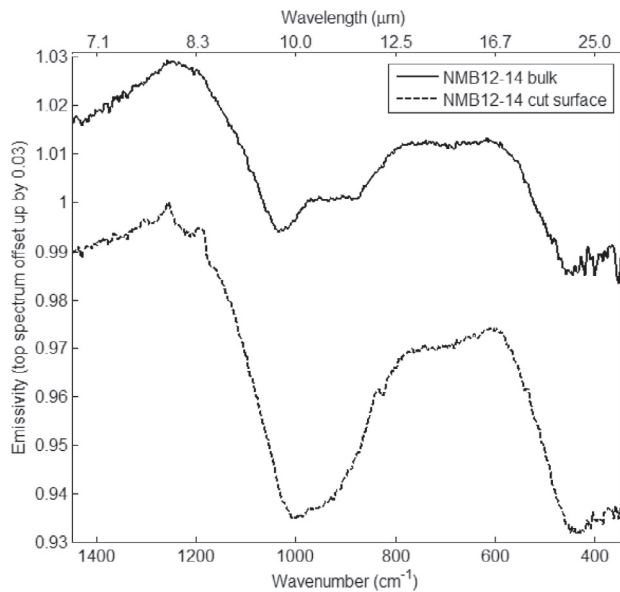


Fig. 6. Emissivity spectra of bulk, relatively undisturbed NMB12-14 glass-rich sample (solid line) and a cut surface (dashed line) on the billet of the sample left over from thin section preparation.

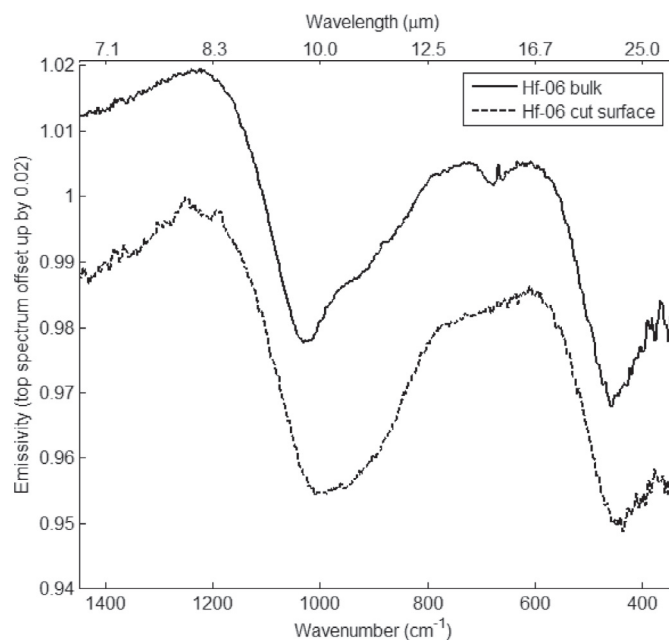


Fig. 7. Emissivity spectra of bulk, relatively undisturbed Hf-06 glass-rich sample (solid line) and a cut surface (dashed line) on the billet of the sample left over from thin section preparation.

feature for both the hydro- and glaciovolcanic glasses and the Lunar crater class-5A and 5B impact melts (Wright et al., 2011). The R^2 of a linear regression through the points is 0.615.

3.2.2. Comparisons of volcanic and impact glasses

Hydro- and glaciovolcanic glasses and impact glasses arise through different processes which have the potential to result in differences in how slowly or rapidly they might devitrify. Glasses formed from impact processes might be quenched rapidly or less rapidly based on their location in the ejecta blanket. Molten material deposited on the top or distal portions of the ejecta blanket would be more prone to rapid quenching while buried melt might not be quenched as quickly. Similarly, in a hydro- or glaciovolcanic

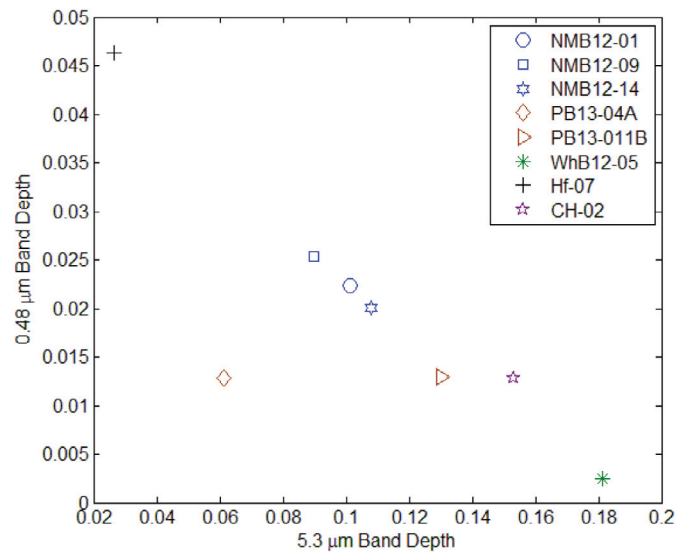


Fig. 8. 0.48 μm band depth (attributed to hematite development) versus 5.3 μm band depth (glass feature).

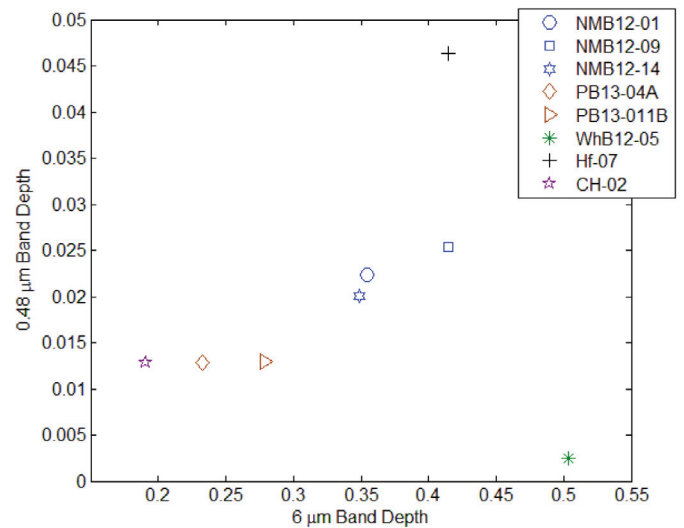


Fig. 9. 0.48 μm band depth (attributed to hematite development) versus 6 μm band depth (attributed to hydration).

setting, a great deal depends on the degree to which ash from the eruption is emplaced “wet” (entrained with steam) or “dry” (steam separated from the ash) or whether the eruption is sub-aqueous (or sub-glacial) or emergent (subaerial) in terms of how rapidly the glass is quenched (Wohletz and Sheridan, 1983).

Wright et al. (2011) described the thermal emissivity spectra of “Class 5” shocked basalt (aka impact melts) produced by the Lunar impact and originally classified by Kieffer et al. (1976). These impact melts differ from unshocked basalt and the lower (Classes 1 through 4) classes of shocked basalt in that nearly all minerals were completely shock-melted to a homogenous black glass (Kieffer et al., 1976). Wright et al. (2011) found that the TIR emissivity spectra of impact melts fall into two spectral categories they labeled Class 5a and Class 5b. The absorption associated with the silica stretching vibration of Class 5a impact melts has an asymmetric “V” shape (steeper slope on the higher wavenumber side of the feature) while the Class 5b impact melt has the double SiO_4 -chain and sheet features described above for hydro- and glaciovolcanic glasses. Fig. 11 compares emissivity spectra of the Hf-06

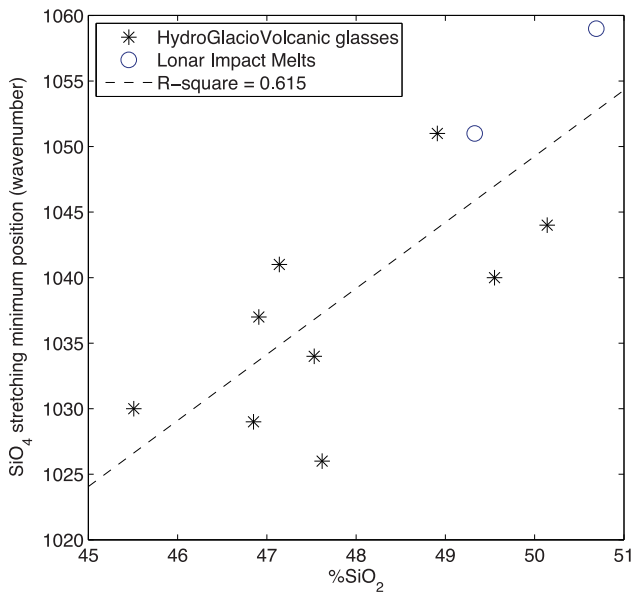


Fig. 10. Plot of the wavenumber minimum of the SiO_4 stretching feature in both Hydro/Glaciovolcanic glass-rich samples versus $\%\text{SiO}_2$ determined from XRF of bulk samples and Lonar crater impact melts. R-square of the line through the points is 0.615.

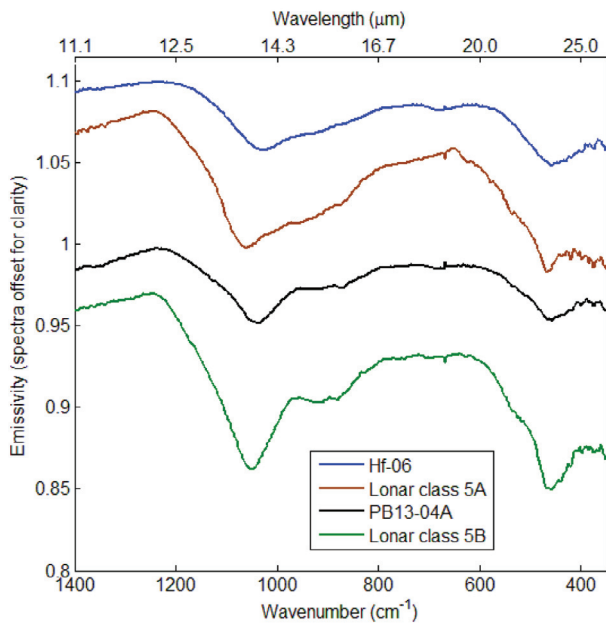


Fig. 11. Comparison of emissivity spectra of glacio- and hydrovolcanic glass-rich samples (Hf-06 and PB13-04A) with the Class 5a and Class 5b impact melts of Wright et al. (2011).

glaciovolcanic and PB13-04A hydrovolcanic minimally altered, glass-rich samples with averages of emissivity spectra of Class 5a and 5b impact melts. In the silica-stretching region, the Hf-06 spectrum resembles the Class-5a spectrum while the PB13-04A spectrum resembles the Class-5b spectrum. As shown in Fig. 1, while having VNIR reflectance spectra with well-defined $1\ \mu\text{m}$ glass bands, the dark, glass-rich Hf-06 and Hf-07 spectra have $1.9\ \mu\text{m}$ water overtone bands. In Figs. 8 and 9, Hf-07 also has higher 0.48 and $6\ \mu\text{m}$ band depths and lower $5.3\ \mu\text{m}$ band depth, indicative of more advanced alteration than other samples it was compared to in those figures. Thus, the resemblance of Class-5a to Hf-06 and Hf-07 indicates it has devitrified more than the Class-

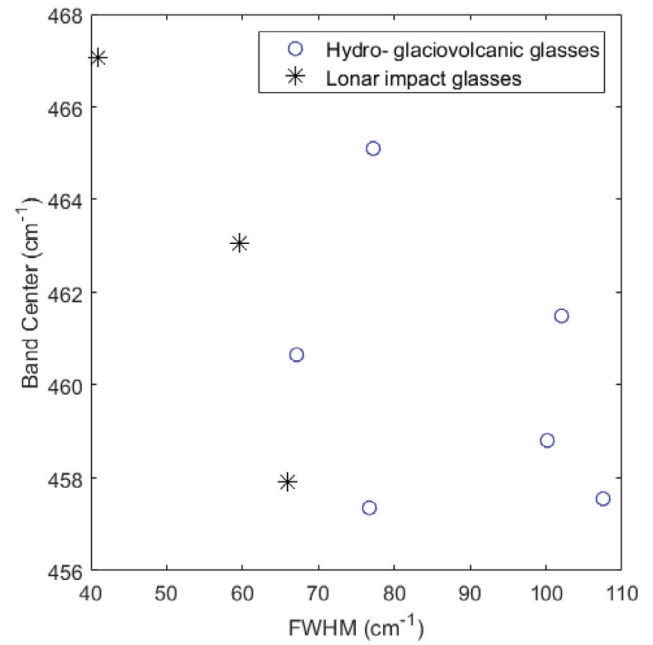


Fig. 12. Plot of the band center position of the Si-bending feature near $462\ \text{cm}^{-1}$ versus the full width at half maximum (FWHM) of that feature for glass-rich spectra from hydro- and glaciovolcanic samples and three Lonar Crater Class 5a and 5b impact melts.

5b impact melt samples. The comparison to TIR spectra of hydrovolcanic glass alteration shown here provides a reason for the differences between the two differing Class 5 impact melt spectra. Limited geochemical comparisons by Wright et al. (2011) between Class 5A and Class 5B did not provide a reason for the spectral differences.

A potential difference between the hydro- and glaciovolcanic glasses and impact glass from Lonar Crater is in the silica bending absorption that is located near $460\ \text{cm}^{-1}$ ($21.7\ \mu\text{m}$). With reference to Fig. 11, this feature is narrower in the Class-5a impact melt spectra than it is for the hydro- and glaciovolcanic glass-rich samples. In the Class-5b spectrum, this feature is again narrower, but less so, than the corresponding feature in the hydro- and glaciovolcanic glass-rich samples. Plotting the band center versus the full-width at half maximum (FWHM) for this feature for hydro- and glaciovolcanic glass-rich and Lonar impact melts, there is no difference in the band center, but Fig. 12 graphically shows the narrower FWHM for the impact melts. The narrower width of the silica bending feature in the Lonar Crater impact melt glasses compared to that in the hydro- and glaciovolcanic glasses is a potential discriminating feature to use in distinguishing hydro- and glaciovolcanic glass from impact melt glass. In general, the bandwidth and shape of MWIR spectral features in silicate glasses are related to the degree of polymerization and overall glass structure (such as the range and proportions of silicate structural units present with the glass; e.g., Dalby and King, 2006). Thus the narrower width of this feature for the impact melts could potentially be ascribed to increased SiO_4 polymerization for those samples. However, given the limited number of impact melt samples, and all from a single crater, we consider this distinction between volcanic and impact glasses a tentative result.

4. Preliminary application to Mars data

Mars analogue sample reflectance and emissivity data is important for understanding the nature of the martian surface as it has been measured in Mars remote sensing datasets. For the analysis

Table 3
Glass-rich emissivity spectra added to deconvolution library.

Sample	Sampling location
NMB12-14 average	N. Menan Butte, Idaho
NMB12-14 cut face average	N. Menan Butte, Idaho
CH-02 average	Crazy Hills, Washington
PB13-011 average	Pavant Butte, Utah

of thermal infrared emissivity data collected by the Thermal Emission Spectrometer (TES) on-board the Mars Global Surveyor (MGS) spacecraft, and for the Mini-TES instrument on-board both Mars Exploration Rovers, an important analysis tool has been the linear deconvolution approach of Ramsey and Christensen (1998). This approach uses a library of laboratory-measured terrestrial sample spectra to form a linear combination of select spectra from that library that best matches the observed TES spectrum with the minimum root mean square (RMS) error. Minitti and Hamilton (2010) used the emissivity spectra of several pristine glasses as library endmembers in the deconvolution of average TES spectra for nine of the eleven regional spectral types determined by Rogers et al. (2007). They found that glass was not required, in fact was not even selected as endmembers, in the deconvolution of any of those regional spectral types. We note however that the glasses that they used were pristine laboratory manufactured glasses. In this paper, we have shown that for even black, minimally hydrated natural glasses of basaltic composition, the SiO₄-sheet and chain features of Crisp et al. (1990) have developed at approximately 9.5 and 11 μm in place of a single U-shaped silica-stretching absorption feature. Thus, running a linear deconvolution using the NNLS deconvolution approach of Rogers and Aharonson (2008) over the 1301–225 cm⁻¹ (7.7–44.4 μm) spectral range with the same library used by Rogers and Christensen (2007) and by Minitti and Hamilton (2010), with the addition of the natural hydrovolcanic glass spectra listed in Table 3 and shown in Fig. 13, we find (as summarized in Table 4) that glass sample spectra can form up to nearly 40% of the N. Acidalia spectral type of Rogers et al. (2007) and constitute significant fractions of several of the other

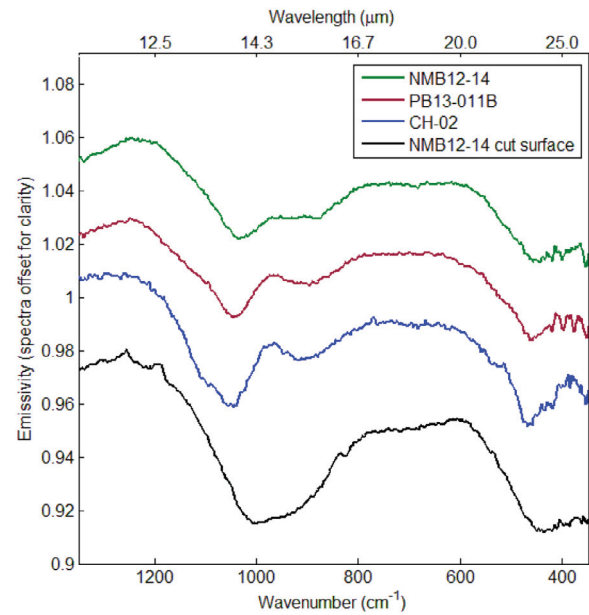


Fig. 13. Emissivity spectra of glass-rich samples used in deconvolution of TES data.

spectral type regions as well. Example measured and modeled TES spectra of the four summary groups of spectral types from Rogers and Christensen (2007) are shown in Fig. 14. Regions that are modeled with over 20% of incipiently devitrified glass (a summation of fractions of those spectra from Table 3) included N. Acidalia, Syrtis Major, Aonium, Mare Sirenum, and Solis Planum. However, while these glass spectra are used as endmembers when included in the endmember library these results are not necessarily “required” by the data; i.e., fits that are nearly as good (as adjudged by RMS error comparisons of measured and modeled spectra) are achievable without including the incipiently devitrified glass-rich spectra (RMS error values of deconvolution without including hydrovolcanic glass sample spectra are shown in the last row of Table 4).

Table 4

Linear deconvolution results for TES spectral types of Rogers et al. (2007) incorporating hydrovolcanic basaltic glass sample spectra. The “shocked” groups are laboratory shocked plagioclase spectra.

EM/group	S Acidalia	N Acidalia	Syrtis	Aonium	Sirenum	Tyrrhena	Meridiani	Cimmeria	Solis	Pandorae
Quartz	0.006	0.012	0.006	0.010	0.006	0.010	0.008	0.008	0.012	0.005
K Feldspar	0.024	0.005	0.015	0.038	0.026	0.029	0.034	0.054	0.032	0.042
Plagioclase	0.209	0.221	0.141	0.185	0.156	0.163	0.175	0.149	0.151	0.169
OPX	0.049	0.090	0.043	0.076	0.047	0.085	0.052	0.089	0.095	0.082
Pigeonite	0.065	0.046	0.015	0.015	0.000	0.044	0.026	0.027	0.096	0.000
CPX	0.084	0.012	0.177	0.143	0.148	0.167	0.191	0.164	0.047	0.136
Olivine	0.000	0.000	0.036	0.016	0.018	0.105	0.081	0.075	0.018	0.042
Mica	0.050	0.012	0.004	0.032	0.013	0.003	0.024	0.013	0.007	0.031
Serpentine	0.000	0.000	0.000	0.000	0.000	0.000	0.000	0.000	0.000	0.000
Phyllos	0.041	0.045	0.004	0.000	0.000	0.000	0.000	0.000	0.000	0.000
Hi Si glass	0.000	0.002	0.000	0.037	0.012	0.041	0.051	0.026	0.017	0.033
Opal	0.012	0.011	0.001	0.003	0.004	0.000	0.005	0.003	0.000	0.010
Amphibole	0.000	0.003	0.019	0.004	0.009	0.003	0.000	0.000	0.008	0.003
Oxide	0.035	0.032	0.000	0.006	0.012	0.010	0.012	0.006	0.027	0.010
Carbonate	0.067	0.024	0.047	0.049	0.048	0.036	0.066	0.047	0.022	0.055
Sulfate	0.104	0.039	0.046	0.094	0.068	0.068	0.096	0.076	0.063	0.099
Zeolite	0.130	0.050	0.072	0.108	0.122	0.107	0.131	0.143	0.107	0.139
Shocked	0.000	0.000	0.070	0.000	0.000	0.000	0.001	0.007	0.088	0.013
CH-02	0.000	0.000	0.000	0.000	0.000	0.000	0.000	0.000	0.013	0.000
NMB12-14	0.000	0.196	0.020	0.000	0.227	0.000	0.000	0.047	0.000	0.049
NMB12-14 cut face	0.000	0.000	0.044	0.185	0.000	0.081	0.047	0.072	0.000	0.083
PB13-011B	0.124	0.2020	0.240	0.000	0.091	0.048	0.000	0.000	0.198	0.000
Hydrovolc glass sum	0.124	0.3981	0.304	0.185	0.318	0.129	0.047	0.119	0.211	0.131
RMS error	0.00,121	0.00,141	0.00,136	0.00,100	0.00,125	0.00,115	0.00,111	0.00,101	0.00,101	0.00,129
RMS error w/o glass	0.00,122	0.00,144	0.00,140	0.00,103	0.00,128	0.00,116	0.00,112	0.00,112	0.00,102	0.00,131

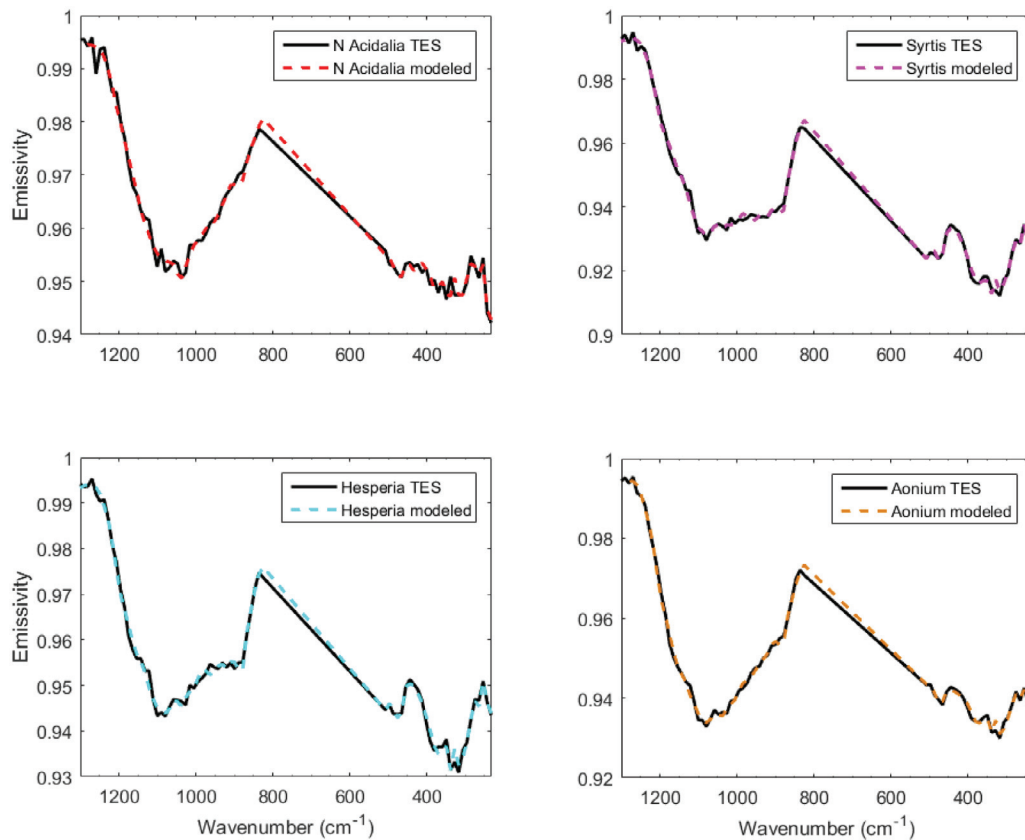


Fig. 14. Atmosphere-removed TES spectra of representatives of Rogers and Christensen (2007) four main spectral groups (black solid lines) compared with modeled spectra using the partially devitrified glass sample spectra in the deconvolution (dashed colored lines).

Table 5

Change in percent of “high silica phases” deconvolution group from Rogers and Christensen (2007) to this study with the inclusion of partially devitrified basaltic glass sample spectra in the deconvolution endmember library.

	N Acidalia	Syrtis	Aonium	Sirenum	Tyrrhena	Hesperia	Meridiani	Cimmeria	Solis
High Si phases, R&C, 2007	34.0	12.0	17.0	21.0	13.0	19.0	22.0	16.0	31.0
High Si phases, this study	7.3	7.3	9.9	12.0	10.9	9.1	10.9	11.9	10.8

One consequence of the inclusion of the partially devitrified basaltic glass spectra in the set of endmember spectra used to model the TES data is not only the role that glass plays as a component of the martian surface layer, but also the effect that its incorporation has on the modeled abundances of other endmember materials. Specifically, we consider the effect on the “high silica phases”. In the modeling of Rogers and Christensen (2007), detailed in Table 2 of that paper, the “high silica phases” group (including amorphous silica, sheet silicates, high silica glasses, and zeolites) ranged from 12 to 34% of the modal mineralogy of the 9 spectral types shown in Table 2 of Rogers and Christensen (2007) with the highest values being in Solis Planum and N. Acidalia (31 and 34% respectively). In our modeling, using the partially devitrified basaltic glass sample spectra, the modeled amount of high silica phases goes down for all the spectral types as shown in Table 5. This is understandable given the similarity of the partially devitrified glass sample spectra to many of the high silica phases spectra (Fig. 15). We interpret the selection of the partially devitrified glass sample spectra over the high silica phases as a geologically reasonable result given the dominance of basaltic volcanism on Mars and the early history of explosive volcanism (e.g., Bandfield et al., 2013) that there would be relatively more (partially devitrified) basaltic glass and less high silica materials. Likewise, given the dominance of

basaltic materials in the martian surface layer, impact melt generated by cratering processes (e.g., Schultz and Mustard, 2004; Cannon and Mustard, 2015) would also be basaltic in composition and nominally similar in its MWIR emissivity to the class 5a and 5b spectra of Wright et al. (2011) and reproduced here in Fig. 11.

5. Discussion

The presence of the SiO_4 -chain and sheet features in even a black, apparently pristine sample such as CH-02, from the Crazy Hills hyaloclastite ridge, indicates that the development of these features is a sensitive indicator of alteration. Thus, if these features do *not* develop in glass-bearing martian surface materials that is indicative of *extremely* low alteration rates. Other spectral indicators of the first stages of alteration include the development of H_2O absorption features at 1.9 and $6\ \mu\text{m}$. The volcanic samples examined are from hydro- and glaciovolcanic centers, thus the tephras were formed in the presence of water and although these minimally altered glass-rich tephras are thought to have been emplaced “dry” (with steam from the eruption having largely separated from the ash cloud; Wohletz and Sheridan, 1983), some fraction of water could have been emplaced with the ash beds leading to the incipient hydration or post-emplacement water

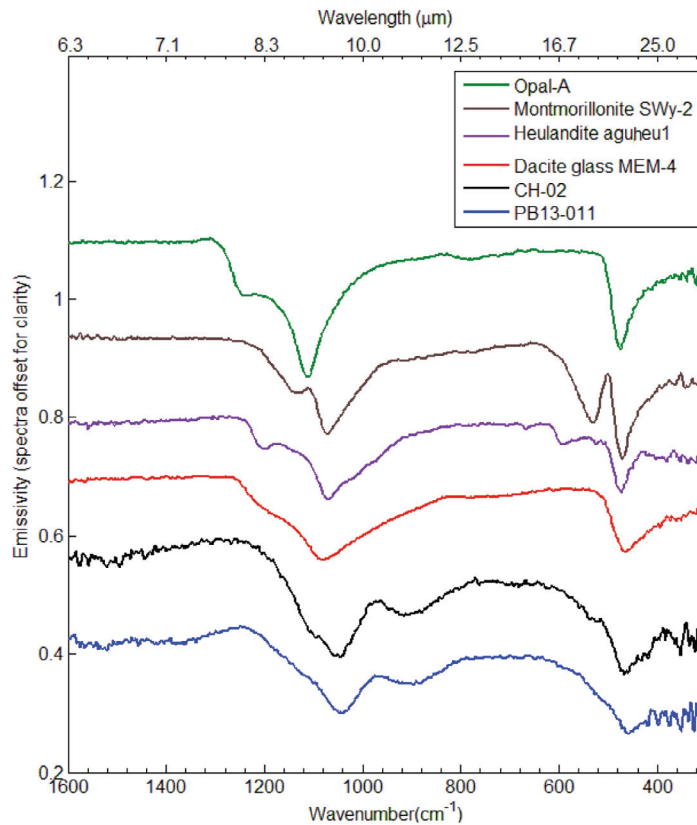


Fig. 15. Comparison of partially devitrified basaltic glass sample spectra (CH-02, PB13-011) with representative “high silica phase” library spectra.

could be responsible. Some level of hydration led to features near $3\ \mu\text{m}$ being nearly ubiquitous, occurring in even the lowest albedo samples. The development of the H_2O bending feature at $6\ \mu\text{m}$ and the bound water overtone feature at $1.9\ \mu\text{m}$ are more sensitive indicators of the first stages of hydration. The first stages of oxidation are indicated by development of a band near $0.48\ \mu\text{m}$, tentatively attributed to hematite.

Impact melt glass and volcanic glass are virtually spectrally indistinguishable. We find minor differences in the shape of the silica bending feature near $450\ \text{cm}^{-1}$ ($22\ \mu\text{m}$) between the glass-rich hydro- and glaciovolcanic sample spectra and average Class-5A and 5B Lobar crater impact melt spectra of Wright et al. (2011). While intriguing, a larger sample size would be required to make a definitive determination as to whether this feature could be reliably used to distinguish between glasses of impact and volcanic origin.

Finally, previous efforts to incorporate basaltic glass emissivity spectra into linear deconvolution of orbital (TES) or surface (Mini-TES) spectra of Mars have used spectra of pristine glasses. In this study we have added several glass-rich sample spectra to the linear deconvolution spectral library used by both Rogers and Christensen (2007) and Minitti and Hamilton (2010) to model the 11 TES spectral classes of Rogers et al. (2007). Bulk sample spectra added to the spectral library evince the early development of the SiO_4 -chain and sheet components of the silica stretching feature. We find that these glass-rich sample spectra are selected by the algorithm to model the TES spectral classes with marginally better RMS error fits than are achieved using a library without these glass-rich sample spectra. The most glass-rich surface type is the N. Acidalia surface type where nearly 40% basaltic hydrovolcanic glass is used to model the TES spectrum. These results are consistent with recent studies such as that of Horgan and Bell (2012) that suggested the presence of abundant glass in the northern plains and results from

lower latitudes from the Spirit and Curiosity rovers that detected the presence of amorphous materials, nominally glass, in observed and sampled materials.

6. Conclusions

Better understanding of the visible to near infrared reflectance and mid-wave infrared emissivity of glasses produced through volcanic and impact processes enable a better ability to consider these materials as possible contributors to the X-ray amorphous component identified in all drill samples to date by CheMin on the Curiosity rover at Gale crater (Downs et al., 2015) and to the potential glass component in rocks at Husband Hill and on Home Plate (Ruff et al., 2006, 2008; Schmidt et al., 2009). In this study, glasses produced by basaltic hydrovolcanic and glaciovolcanic activity at a number of terrestrial field sites as well as impact melts from the basaltic Lobar Crater in India have been examined using thin section petrography, visible and near infrared reflectance and mid-wave infrared emission spectroscopy.

The reflectance characteristics of the most glass-rich samples (as determined from thin section petrography and visual inspection) in the 0.3 to $2.6\ \mu\text{m}$ range resemble those reported in previous studies of basaltic glasses (Dyar and Burns, 1982; Farrand and Singer, 1992; Minitti et al., 2002) with broad Fe crystal field bands centered near 1 and $2\ \mu\text{m}$. Biconical reflectance measured at longer wavelengths (0.83 – $25\ \mu\text{m}$) indicated the presence of a glass band at $5.32\ \mu\text{m}$, which weakens in samples with increasing alteration (as measured by the growth of the water bending vibration at $6.1\ \mu\text{m}$ and Fe^{3+} feature at $0.48\ \mu\text{m}$).

The MWIR character of these samples (measured in both reflectance and emissivity, but reported here in terms of emissivity) was found to vary based on the incipient devitrification of the samples. Glass grains in thin section examined by a micro-FTIR

instrument have the broad “U” shaped feature of fresh basaltic glass in the 9–10 μm region as do the cut surfaces of the billets left by thin section creation. However, natural sample surfaces have a narrow feature centered near 9.5–9.6 μm and a weaker, broader feature centered near 10.9–11.3 μm . These features correspond to the “B” and “C” features described by Crisp et al. (1990) which were interpreted by those authors as resulting from the development of SiO_4 sheet and chain structures respectively.

Also prominent in the MWIR range of all of these glass-rich samples is a SiO_4 bending feature centered near 21.3–22.2 μm . Comparing this feature in the hydro- and glaciovolcanic glasses to that in the Class 5a and 5a Loner Crater impact melt spectra of Wright et al. (2011) indicates that this feature is broader in the former samples than in the latter. While this feature could potentially be used to discriminate between volcanic and impact glasses, we suggest that examination of more samples is required to fully validate this conclusion.

Noting that the SiO_4 chain and sheet spectral features are observed in samples that appear fresh by visual inspection and even by the criteria of having minimal hydration features at 1.9 and 6.1 and little oxidation as adjudged by the lack of a 0.48 μm band, we suggest that using spectra with these features would be a better library endmember for MWIR linear deconvolutions (Ramsey and Christensen, 1998) than the spectra of pristine basaltic glasses. A preliminary deconvolution analysis of the 11 martian surface TES spectral types of Rogers et al. (2007) using hydro- and glaciovolcanic glass sample spectra as endmembers indicated that all of the examined units had some glass component and that N. Acidalia, already noted by Horgan and Bell (2012) as having a significant glass component based on VNIR spectral studies, had close to 40% of these basaltic hydrovolcanic partially devitrified glasses. Incorporation of the partially devitrified glasses into the deconvolution led to the drop in modeled abundance of the high silica phases group. The presence of basaltic glasses instead of high silica phases is consistent with our knowledge of Mars as being predominantly basaltic and the possibility of these being hydro- or glaciovolcanically derived glasses is consistent with abundant water or ice/volcano interactions early in Mars' history (Allen, 1979; Squyres et al., 1987; Head and Wilson, 2002). Further study is required to assess the role of incipient glass devitrification under ambient conditions, as examined here, and alteration of glasses under acidic conditions as discussed by Smith et al. (2014). More detailed analyses should highlight additional glass-rich regions and different types of glasses based on the endmembers selected by the analysis. However, we note that while the deconvolutions selected the glass sample spectra as endmembers, the fits, indicated by a RMS error metric were better, but not greatly better, than deconvolutions performed without the glass sample spectra.

Additional study of the TES spectral types and nominally glass-rich materials observed with the Mini-TES instrument of the Spirit rover are expected to improve our understanding of the significance of a glass component in the martian surface layer.

Acknowledgments

This work was funded by the NASA Mars Fundamental Research Program grant number NNX12AH92G. We thank V. Hamilton of SWRI and M. Osterloo of LASP for sample measurements. Thanks to Kevin Cannon and an anonymous reviewer for helpful reviews.

References

Adams, J.B., Smith, M.O., Gillespie, A.R., 1993. Imaging spectroscopy: Interpretation based on spectral mixture analysis. In: Pieters, C.M., Englert, P.A.J. (Eds.), *Remote Geochemical Analysis: Elemental and Mineralogical Composition*. Cambridge University Press, New York, pp. 145–166.

- Allen, C.C., 1979. Volcano-ice interactions on Mars. *J. Geophys. Res.: Solid Earth* 84, 8048–8059.
- Bandfield, J.L., Edwards, C.S., Montgomery, D.R., Brand, B.D., 2013. The dual nature of the martian crust: Young lavas and old clastic materials. *Icarus* 222, 188–199.
- Brand, B.D., White, C.M., 2007. Origin and stratigraphy of phreatomagmatic deposits at the Pleistocene Sinkler Butte Volcano, Western Snake River Plain, Idaho. *J. Volcanol. Geotherm. Res.* 160, 319–339.
- Cannon, K.M., Mustard, J.F., 2015. Preserved glass-rich impactites on Mars. *Geology* 43, 635–638.
- Christensen, P.R., et al., 2000. A thermal emission spectral library of rock-forming minerals. *J. Geophys. Res.* 105 (E4), 9735–9739.
- Clark, R.N., 1999. Chapter 1: spectroscopy of rocks and minerals, and principles of spectroscopy. In: Rencz, A.N. (Ed.), *Manual of Remote Sensing, Volume 3, Remote Sensing for the Earth Sciences*. John Wiley and Sons, New York, pp. 3–58.
- Creighton, D.N., 1987. Menan Buttes, southeastern Idaho. In: *Geological Society of America Centennial Field Guide- Rocky Mountain Section*, pp. 109–111.
- Crisp, J., Kahle, A.B., Abbott, E.A., 1990. Thermal infrared spectral character of Hawaiian basaltic glasses. *J. Geophys. Res.* 95 (21), 621–657 669.
- Dalby, K.N., King, P.L., 2006. A new approach to determine and quantify structural units in silicate glasses using micro-reflectance Fourier-Transform infrared spectroscopy. *Am. Mineral.* 91, 1783–1793.
- Downs, R.T., the MSL Science Team, 2015. Determining mineralogy on Mars with the CheMin X-ray diffractometer. *Elements* 11 (1), 45–50. doi:10.2113/gselements.11.1.45.
- Dyar, M.D., Burns, R.G., 1982. Coordination chemistry of iron in glasses contributing to remote-sensed spectra of the moon. In: *Lunar and Planetary Science Conference Proceedings*, 12, pp. 695–702.
- Farmer, V.C. (1974) *The Infrared Spectra of Minerals*, Mineralogical Society, 539 pp.
- Farrand, W.H. (1991) Visible and near infrared reflectance of tuff rings and tuff cones, PhD Dissertation, University of Arizona, 187 pp.
- Farrand, W.H., Singer, R.B., 1992. Alteration of hydrovolcanic basaltic ash: Observations with visible and near-infrared spectrometry. *J. Geophys. Res.* 97 (17), 317–393 408.
- Fredriksson, K., Dube, A., Milton, D.J., Balasundaram, M.S., 1973. Lonar Lake, India: an impact crater in basalt. *Science* 180 (4088), 862–864.
- Hammond, P., 1987. Lone Butte and Crazy Hills: Subglacial volcanic complexes, Cascade Range. In: *GSA Centennial Field Guide- Cordilleran Section*. Washington, pp. 339–344.
- Head, J.W., Wilson, L., 2002. Mars: a review and synthesis of general environments and geological settings of magma-H₂O interactions. *Geol. Soc. London, Spec. Publ.* 202, 27–57.
- Horgan, B., Bell III, J.F., 2012. Widespread weathered glass on the surface of Mars. *Geology* 40, 391–394. doi:10.1130/G32755.1.
- Kieffer, S.W., Schaal, R.B., Gibbons, R., Horz, F., Milton, D.J., Dube, A., 1976. 7th Lunar Science Conference, Houston, Texas, USA, pp. 1391–1412.
- King, P.L., McMillan, P.F., Moore, G.M., 2004. Infrared spectroscopy of silicate glasses with application to natural systems. In: King, P.L., Ramsey, M.S., Swayze, G.A. (Eds.), *Infrared Spectroscopy in Geochemistry, Exploration Geochemistry, and Remote Sensing*, 33. Mineral. Assoc. Canada, Short Course Series, pp. 93–133.
- Kruse, F.A., Lefkoff, A.B., Boardman, J.W., Heidebrecht, K.B., Shapiro, A.T., Barloon, P.J., Goetz, A.F.H., 1993. The spectral image processing system (SIPS) – Interactive visualization and analysis of imaging spectrometer data. *Remote Sens. Environ.* 44, 145–164.
- Maloof, A.C., Stewart, S.T., Weiss, B.P., Soule, S.A., Swanson-Hysell, N.L., Louzada, K.L., Poussart, P.M., 2010. Geology of Lonar Crater, India. *Geol. Soc. Am. Bull.* 122, 109–126.
- Minitti, M.E., Mustard, J.F., Rutherford, M.J., 2002. Effects of glass content and oxidation on the spectra of SNC-like basalts: Applications to Mars remote sensing. *J. Geophys. Res.* 107 (E5). doi:10.1029/2001JE001518.
- Minitti, M.E., Hamilton, V.E., 2010. A search for basaltic-to-intermediate glasses on Mars: Assessing martian crustal mineralogy. *Icarus* 210, 135–149.
- Pieters, C.M., Mustard, J.F., Sunshine, J.M., 1996. Quantitative mineral analyses of planetary surfaces using reflectance spectroscopy. In: Dyar, M.D., McCammon, C., Schaefer, M.W. (Eds.), *Mineral Spectroscopy: A Tribute to Roger G. Burns*. Geochemical Society, 5, Houston, TX, pp. 307–325.
- Ramsey, M.S., Christensen, P.R., 1998. Mineral abundance determination: Quantitative deconvolution of thermal emission spectra. *J. Geophys. Res.* 103, 577–596.
- Rogers, A.D., Christensen, P.R., 2007. Surface mineralogy of Martian low-albedo regions from MGS-TES data: Implications for upper crustal evolution and surface alteration. *J. Geophys. Res.* 112, E01003. doi:10.1029/2006JE002727.
- Rogers, A.D., Bandfield, J.L., Christensen, P.R., 2007. Global spectral classification of Martian low-albedo regions with Mars Global Surveyor Thermal Emission Spectrometer (MGS-TES) data. *J. Geophys. Res.* 112, E02004. doi:10.1029/2006JE002726.
- Rogers, A.D., Aharonson, O., 2008. Mineralogical composition of sands in Meridiani Planum determined from Mars exploration rover data and comparison to orbital measurements. *J. Geophys. Res.* 113, E06S14. doi:10.1029/2007JE002995.
- Ruff, S.W., Christensen, P.R., Barbera, P.W., Anderson, D.L., 1997. Quantitative thermal emission spectroscopy of minerals: A laboratory technique for measurement and calibration. *J. Geophys. Res.* 102 (14), 814–899. doi:10.1029/97JB00593, 913.
- Ruff, S.W., Christensen, P.R., Blaney, D.L., Farrand, W.H., Johnson, J.R., Michalski, J.R., Moersch, J.E., Wright, S.P., Squyres, S.W., 2006. The rocks of Gusev Crater as viewed by the Mini-TES instrument. *J. Geophys. Res.* 111, E12S18. doi:10.1029/2006JE002747.

- Ruff, S.W., Christensen, P.R., Glotch, T.D., Blaney, D.L., Moersch, J.E., Wyatt, M.B., 2008. The mineralogy of Gusev crater and Meridiani Planum derived from the miniature thermal emission spectrometers on the spirit and opportunity rovers. In: Bell, III, J.F. (Ed.), *The Martian Surface: Composition, Mineralogy, and Physical Properties*. Cambridge University Press, New York, pp. 315–338.
- Schmidt, M.E., et al., 2009. Spectral mineralogical, and geochemical variations across Home Plate, Gusev Crater, Mars indicate high and low temperature alteration. *Earth and Planet. Sci. Lett.* 281, 258–266.
- Schopka, H.H., Gudmundsson, M.T., Tuffen, H., 2006. The formation of Helgafell, southwest Iceland, a monogenetic subglacial hyaloclastite ridge: Sedimentology, hydrology and volcano-ice interaction. *J. Volcanol. Geotherm. Res.* 152, 359–377.
- Schultz, P.H., Mustard, J.F., 2004. Impact melts and glasses on Mars. *J. Geophys. Res.* 109, E01001. doi:10.1029/2002JE002025.
- Smith, R.J., Horgan, B., Christensen, P.R., Mann, P., Cloutis, E.A., 2014. Acid alteration of basalts: Thermal infrared spectra and implications for high silica phases on Mars. In: *45th Lunar and Planet. Sci. Conf.*
- Squyres, S.W., Wilhelms, D.E., Moosman, A.C., 1987. Large-scale volcano-ground ice interactions on Mars. *Icarus* 70, 385–408.
- White, J.D.L., 1996. Pre-emergent construction of a lacustrine basaltic volcano, Pahvant Butte, Utah (USA). *Bull. Volcanol.* 58, 249–262.
- Wohletz, K.H., Sheridan, M.F., 1983. Hydrovolcanic explosions II. Evolution of basaltic tuff rings and tuff cones. *Am. J. Sci.* 283, 385–413.
- Womer, M.B., 1977. The origin of Split Butte: A maar type crater of the south-central Snake River Plain, Idaho. In: Greeley, R., King, J.S. (Eds.), *Volcanism of the Eastern Snake River Plain, Idaho*, pp. 190–202 NASA CR-154621.
- Wright, S.P., Christensen, P.R., Sharp, T.G., 2011. Laboratory, thermal emission spectroscopy of shocked basalt from Lonar Crater, India, and implications for Mars orbital and sample data. *J. Geophys. Res.* 116, E09006. doi:10.1029/2010JE003785.